

Generation of Training Data by Degradation Models for Traffic Sign Symbol Recognition

Hiroyuki ISHIDA^{†a)}, Student Member, Tomokazu TAKAHASHI[†], Ichiro IDE[†], Yoshito MEKADA^{††}, and Hiroshi MURASE[†], Members

SUMMARY We present a novel training method for recognizing traffic sign symbols. The symbol images captured by a car-mounted camera suffer from various forms of image degradation. To cope with degradations, similarly degraded images should be used as training data. Our method artificially generates such training data from original templates of traffic sign symbols. Degradation models and a GA-based algorithm that simulates actual captured images are established. The proposed method enables us to obtain training data of all categories without exhaustively collecting them. Experimental results show the effectiveness of the proposed method for traffic sign symbol recognition.

key words: traffic sign recognition, generative learning method, genetic algorithm, car-mounted camera

1. Introduction

Technologies for supporting drivers with car-mounted cameras have gained considerable industrial interest in recent years. There have been studies on pedestrian detection [1], traffic signal recognition [2], and rain drop detection for the automatic control of wipers [3]. Traffic sign recognition is another important task. If such a recognition system comes into practice, it could support drivers by informing them of the current speed limit, for instance. Also, it could be applicable for periodically updating road map databases used for navigation. The two main issues in traffic sign recognition are detection and classification. Various attempts have been carried out on the detection of traffic signs: edge detection mask [4], hierarchical template [5], shape information [6], and color information [7]. There have also been methods proposed specifically for circular sign detection [8], [9]. [10] and [11] present methods for shape classification. On the other hand, relatively few studies have been conducted on the category classification of extracted signs. Furthermore, most are mainly oriented toward high-quality images. In [12], results from high-quality images are preferentially used for avoiding degradations. A method specializing in speed sign classification [13] copes with the rotation of traffic sign symbols. However, few studies have focused on the various degradations appearing in camera-captured images. This paper focuses on the classification of degraded

traffic sign symbols.

Image degradation is a challenging problem in classifying traffic sign symbols captured by a car-mounted camera. Paclik et al. [14] evaluated similarities in several regions located on a traffic sign plate to solve partial occlusion or deflection problem. Importantly, any method that evaluates similarity needs template images as training data. To recognize symbols with degradations, training data should be captured under similar conditions. However, it is actually difficult and unpractical to collect such training data for all categories. In this paper, we propose a method that automatically generates training data in accordance with actual degradation characteristics. Defining generation parameters enables us to simulate degraded images; combining these parameters produces a large variety of training data. The proposed training method estimates parameter distribution from captured images. For this purpose, a set of generation parameters is estimated for each image by Genetic Algorithm (GA) [15]. Once parameter distribution is estimated, training data following the estimated degradation characteristics are generated for all categories. One main benefit of this method is that training data of all categories can be generated from their original templates, applying the degradation characteristics obtained from captured images, even of a different category. The recognition step is based on the subspace method [16].

This paper is organized as follows: Section 2 introduces the generation parameters. In Sect. 3, the proposed training method is introduced, and in Sect. 4, recognition step is described. Results are presented in Sect. 5.

2. Degradation Models

Training data are generated from an original image by three degradation models: rotation, blurring, and segmentation error. These models are defined with generation parameters, as shown in Fig. 1. Given a CG image P_0 of a traffic sign symbol, degraded image P_3 is generated from P_0 as described below:

1. Rotation

This model simulates the rotation of traffic signs. Assume that the original traffic sign plate exists in plane $z = 0$, and its center is at point $(0, 0, 0)$. Rotation angle parameters are denoted as θ_x , θ_y , and θ_z , and the rotation matrices around each axis are denoted as \mathbf{R}_x , \mathbf{R}_y ,

Manuscript received October 2, 2006.

Manuscript revised February 8, 2007.

[†]The authors are with the Graduate School of Information Science, Nagoya University, Nagoya-shi, 464-8603 Japan.

^{††}The author is with Life System Science and Technology, Chukyo University, Toyota-shi, 470-0393 Japan.

a) E-mail: hishi@murase.m.is.nagoya-u.ac.jp

DOI: 10.1093/ietisy/e90-d.8.1134

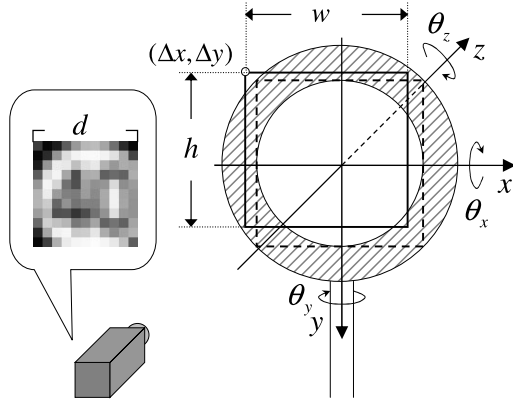


Fig. 1 Parameters for degradation models.

and R_z . The rotation operation is represented as

$$P_1(x, y) = P_0(x', y') \quad (1)$$

with

$$\begin{bmatrix} x' \\ y' \\ z' \end{bmatrix} = (\mathbf{R}_z(\theta_z)\mathbf{R}_y(\theta_y)\mathbf{R}_x(\theta_x))^{-1} \begin{bmatrix} x \\ y \\ 0 \end{bmatrix}, \quad (2)$$

where

$$\mathbf{R}_x(\theta_x) = \begin{bmatrix} 1 & 0 & 0 \\ 0 & \cos \theta_x & -\sin \theta_x \\ 0 & \sin \theta_x & \cos \theta_x \end{bmatrix} \quad (3)$$

$$\mathbf{R}_y(\theta_y) = \begin{bmatrix} \cos \theta_y & 0 & \sin \theta_y \\ 0 & 1 & 0 \\ -\sin \theta_y & 0 & \cos \theta_y \end{bmatrix} \quad (4)$$

$$\mathbf{R}_z(\theta_z) = \begin{bmatrix} \cos \theta_z & -\sin \theta_z & 0 \\ \sin \theta_z & \cos \theta_z & 0 \\ 0 & 0 & 1 \end{bmatrix}. \quad (5)$$

2. Blurring

The model of blurring is assumed as convolution with the Gaussian function, and thereby this model is controlled by a single Gaussian parameter γ . This blurring operation is represented using convolution (*) as

$$P_2(x, y) = P_1(x, y) * \left[\frac{1}{2\pi\gamma^2} \exp\left(-\frac{x^2 + y^2}{2\gamma^2}\right) \right]. \quad (6)$$

3. Segmentation error

This model is used to simulate incorrectly segmented symbol images. Horizontal and vertical gap parameters $(\Delta x, \Delta y)$, segmented area parameters (w, h) , and segmented image size d are introduced. P_3 is represented as

$$P_3(i, j) = \frac{1}{|D_{(i,j)}|} \sum_{x,y \in D_{(i,j)}} P_2(x, y), \quad (7)$$

where $D_{(i,j)}$ is a set of pixels projected on pixel $P_3(i, j)$ and represented as

$$D_{(i,j)} = \left\{ (x, y) \mid \frac{i}{d+1}w \leq x - \Delta x < \frac{i+1}{d+1}w, \right. \\ \left. \frac{j}{d+1}h \leq y - \Delta y < \frac{j+1}{d+1}h \right\}. \quad (8)$$

3. Training by Generative Learning

The generative learning method was developed to reproduce synthetic degraded patterns by simulating actual degradation [17]. In contrast with the collection-based approach, the generative learning method eliminates the exhaustive collection of training data. Traditionally, this approach has often been used for learning distorted characters in handwritten character recognition [18], [19]. We have been applying generation-based approaches to camera-based character recognition [20], [21]. They enable us to acquire parametrically degraded character images in accordance with actual degradations. However, they cannot be directly applied to traffic sign symbol recognition. In [20], it is assumed that a character is located at the center of the image and that a camera looks perpendicularly at the target document. Also [21] failed to discuss how to determine the values of parameters in the generation step. From the viewpoint of generating training sets for the analysis of principal components (PCA), training sets with various levels of degradation are needed [22]. Furthermore, a range of the levels should be adequately determined. Using the degradation models in Sect. 2, the proposed method estimates it from actually captured images, assuming that the estimated parameter range is suited to recognize traffic signs captured in similar conditions. To represent the parameter range, a multivariational normal distribution is used for approximation. It provides a simple and generally applicable framework, in which parameter range can be controlled by mean and variance. Once the parameter distribution is obtained, the degradation models allow us to reproduce the learned degradation characteristics. This is possible for any category of traffic sign symbols because the degradation models are applicable universally to them. Recall that capturing the training data of all categories is extremely difficult in traffic sign recognition. The major advantage of the proposed method is that the training data of almost all categories can be replaced by the generated data.

This method consists of two steps. The first is the parameter estimation step introduced in 3.1. The second is the generation step introduced in 3.2.

3.1 Parameter Estimation Step

Distribution of generation parameters is estimated from actual images, which are used to simulate degradations. The parameters for each image need to be estimated to calculate distribution. These images should be captured by the same imager as that used in the recognition step. It is also required to exclude the images which looks obviously unsuitable for the parameter estimation. If degradation characteristics of

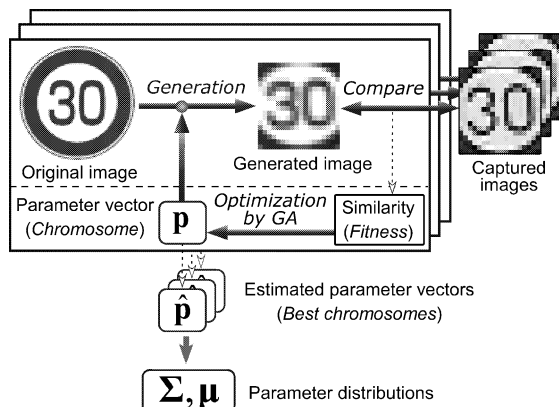


Fig. 2 Parameter estimation step.

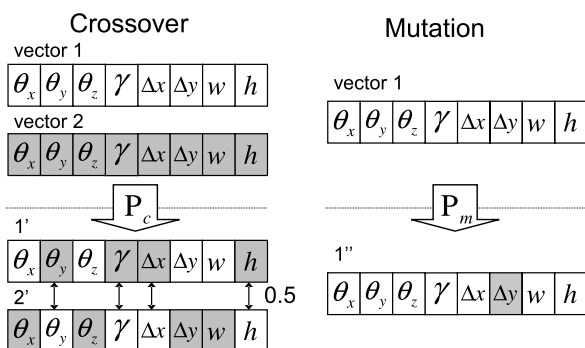


Fig. 3 Operations used in genetic algorithm.

the images are dissimilar to the general ones, the training will not be successful. Parameter vector \mathbf{p} consisting of the generation parameters introduced in Sect. 2 is defined as:

$$\mathbf{p} = (\theta_x, \theta_y, \theta_z, \gamma, \Delta x, \Delta y, w, h). \quad (9)$$

This vector is used to generate a degraded image from an original image. Figure 2 illustrates this estimation step. Let T be one of the captured images for parameter estimation and Q be an image generated from the original image of T with \mathbf{p} . Parameter vector $\hat{\mathbf{p}}$, which maximizes similarity between Q and T , should be found and accepted as the optimal representation of the degradation characteristics of T . The similarity between these two images is defined as inner product $\langle \mathbf{q}, \mathbf{t} \rangle$, where \mathbf{q} and \mathbf{t} are constructed from the pixel values of images Q and T , respectively. Simultaneously, each vector is normalized such that the average of its elements is 0 and the norm is 1, namely, $\langle \mathbf{q}, \mathbf{q} \rangle = 1$ and $\langle \mathbf{t}, \mathbf{t} \rangle = 1$. Figure 3 illustrates the crossover and mutation operations. A detailed description of the GA-based parameter estimation algorithm is given in Appendix. Table 1 lists parameters for the GA. Figure 4 shows an example of captured image t and simulated images by GA.

Parameter distribution is estimated from multiple parameter vectors $\hat{\mathbf{p}}$ computed from captured images. Average vector $\boldsymbol{\mu}$ and covariance matrix $\boldsymbol{\Sigma}$ are then obtained from the multiple vectors $\hat{\mathbf{p}}$ by

$$\boldsymbol{\mu} = \mathcal{E}[\hat{\mathbf{p}}], \quad (10)$$

Table 1 Parameters for genetic algorithm.

N_c	Population size
G	Number of generations
P_c	Crossover rate
P_m	Mutation rate

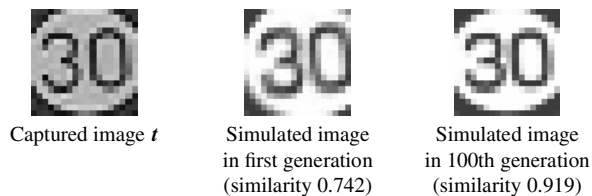


Fig. 4 Simulated images for captured image.

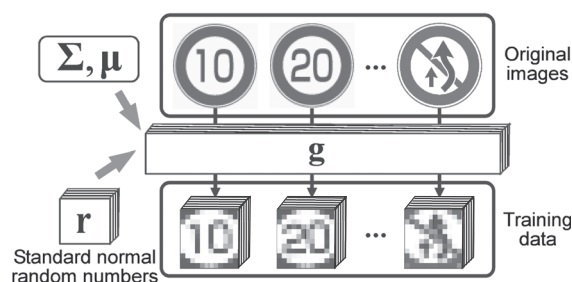


Fig. 5 Generation of training data.

$$\boldsymbol{\Sigma} = \mathcal{E}[(\hat{\mathbf{p}} - \boldsymbol{\mu})(\hat{\mathbf{p}} - \boldsymbol{\mu})^t]. \quad (11)$$

Note that size parameter d is not contained in \mathbf{p} because d can be obtained directly from each captured image itself. The value of d is set equal to the size of the captured image in the GA-based parameter estimation algorithm. Also for avoiding complexity, this method assumes that d is independent of the other parameters; $\boldsymbol{\mu}$ and $\boldsymbol{\Sigma}$ are computed without regard to d .

3.2 Generation Step

Once parameter distribution is estimated, parameter vector \mathbf{g} , which follows the estimated distribution, is produced from $\boldsymbol{\mu}$ and $\boldsymbol{\Sigma}$ by the following parameter-producing function:

$$\mathbf{g} = \boldsymbol{\Sigma}^{1/2} \mathbf{r} + \boldsymbol{\mu}, \quad (12)$$

where \mathbf{r} denotes a vector composed of standard normal random numbers [23] and $\boldsymbol{\Sigma}^{1/2}$ denotes the Cholesky decomposition [24] of $\boldsymbol{\Sigma}$. Figure 5 illustrates this generation step. Various parameter vectors are produced, and correspondingly, various training data of all categories and sizes are generated.

4. Recognition Method

The subspace method [16] is used in the recognition step. The process of constructing a subspace is described in 4.1,



Fig. 6 Top three eigenvectors. (Speed limit 20 km/h, size 16×16)

followed by a description of the recognition step using multiple-frame integration in 4.2. Although this research does not focus on the extraction of traffic signs, extraction methods need to be used to evaluate the proposed training method. A simple algorithm to extract round traffic signs is introduced in 4.3.

4.1 Construction of a Subspace

A subspace is constructed from the generated training data for each category and also for each size.

Let $\mathbf{x}_{\{n,d\}}^{(c)}$ be a vector consisting of $d \times d$ pixels of category c 's n -th training data whose size is d ; $\mathbf{x}_{\{n,d\}}^{(c)}$ is normalized so that its norm is 1, and the average of its elements is 0. Eigenvectors are constructed for each category c and for each size d . Initially matrix $\mathbf{X}_d^{(c)}$ is constructed from N training data ($n = 1, \dots, N$) by

$$\mathbf{X}_d^{(c)} = \begin{bmatrix} \mathbf{x}_{\{1,d\}}^{(c)} & \dots & \mathbf{x}_{\{N,d\}}^{(c)} \end{bmatrix}. \quad (13)$$

Auto-correlation matrix $\mathbf{Q}_d^{(c)}$ is computed by

$$\mathbf{Q}_d^{(c)} = \mathbf{X}_d^{(c)} (\mathbf{X}_d^{(c)})^t. \quad (14)$$

Eigenvectors are derived from $\mathbf{Q}_d^{(c)}$, of which $\mathbf{e}_{\{l,d\}}^{(c)}$ ($l = 1, \dots, L$) with the largest L ($< N$) eigenvalues are used for recognition. Figure 6 shows examples of the eigenvectors. The reason why the subspaces are constructed for each size is that size normalization can have an undesirable effect on the matching process. If the size normalization is used, the influence of pixel interpolation on very small images is not negligible.

4.2 Multiple Frame Integration

A given image is classified to category c that maximizes similarity, which is defined as the sum of the squared inner product between the given image and the eigenvectors. Yanadume et al. demonstrated that integrating similarity from multiple frames improves recognition accuracy [25]. Given M image frames of the same target, let \mathbf{z}_m be a vector normalized identically as the training data from the m -th image ($m = 1, \dots, M$); the recognition result is obtained by

$$\hat{c} = \arg \max_c \sum_{m=1}^M \sum_{l=1}^L \left\langle \mathbf{e}_{\{l,\bar{d}_m\}}^{(c)}, \mathbf{z}_m \right\rangle^2, \quad (15)$$

where \bar{d}_m represents the size of segmented image \mathbf{z}_m . In order to distinguish it from size parameter d in the generation step, size of captured images is denoted as \bar{d} .

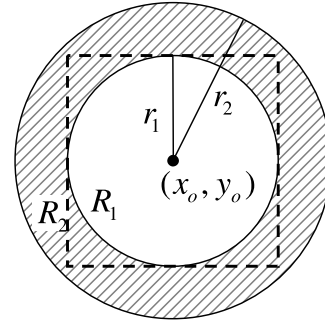


Fig. 7 Segmentation parameters for a round sign.

4.3 Round Sign Detection

HSV color space [26] is useful to extract symbol regions in round signs, since H and S are nearly uniform in respect to changes of illumination. Let a discriminant function for finding the red circumference be defined as

$$\text{red}(x, y) = \begin{cases} 1 & \left(\begin{array}{l} -\pi/9 < H(x, y) < \pi/9 \\ \text{and } 0.2 < S(x, y) \leq 1 \\ \text{and } 30 \leq V(x, y) \leq 255 \end{array} \right) \\ 0 & \text{otherwise} \end{cases}. \quad (16)$$

Round signs can be detected by matching a doughnut-shaped structure shown with segmentation parameters in Fig. 7. Here (x_0, y_0) is the center point, R_1 is the symbol area, R_2 is the red circumferential area, and r_1 and r_2 are the radii of R_1 and R_2 , respectively. They are represented as

$$R_1 = \left\{ (x, y) \mid \sqrt{(x - x_0)^2 + (y - y_0)^2} < r_1 \right\} \quad (17)$$

and

$$R_2 = \left\{ (x, y) \mid r_1 < \sqrt{(x - x_0)^2 + (y - y_0)^2} < r_2 \right\}. \quad (18)$$

The area to be segmented is the smallest square that includes the entire symbol area. Using Eqs. (16), (17), and (18), segmentation parameters (x_0, y_0) and segmented image size \bar{d} are obtained by

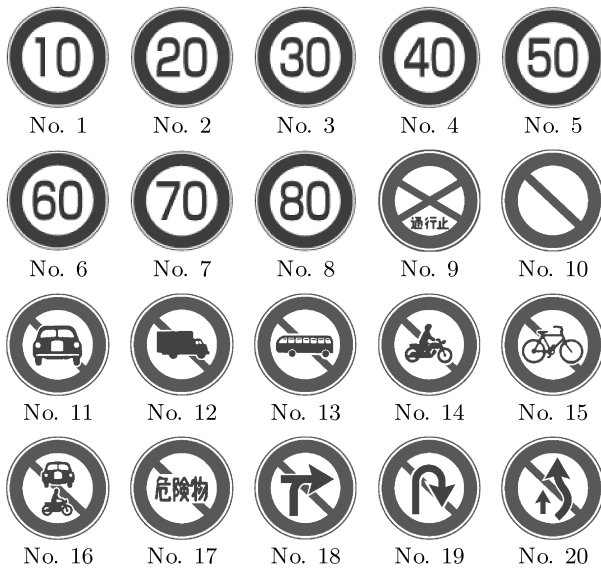
$$\left\{ x_0, y_0, \frac{\bar{d}}{2} \right\} = \arg \max_{\{x,y,r_1\}} \left[\sum_{(x,y) \in R_2} \frac{\text{red}(x, y)}{|R_2|} - \sum_{(x,y) \in R_1} \frac{\text{red}(x, y)}{|R_1|} \right]. \quad (19)$$

5. Experiment

An experiment was performed using video data captured by a car-mounted camera (Table 2) during one run on a sunny morning. Figure 8 illustrates twenty round traffic signs commonly used in Japan. The video data contained fifteen traffic signs: two of No.2, five of No.4, three of No.5, three of No.12, and two of No.20. They were divided into five data sets of each category, with the intent to ascertain whether a

Table 2 Specifications of car-mounted camera.

Product model	Sony DCR-PC105
Resolution	720 × 480
Frame rate	30 fps
Focus length	3.7 mm

**Fig. 8** Traffic sign categories.**Table 3** Number of symbol images in each data set.

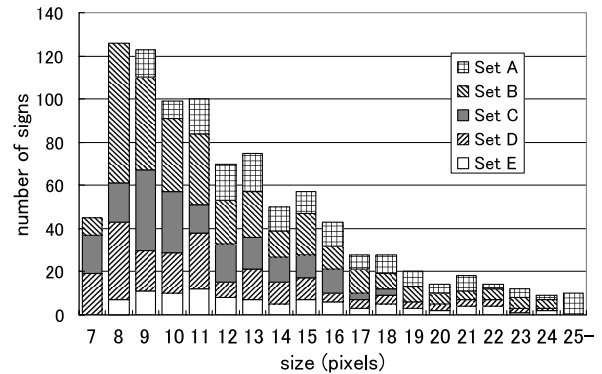
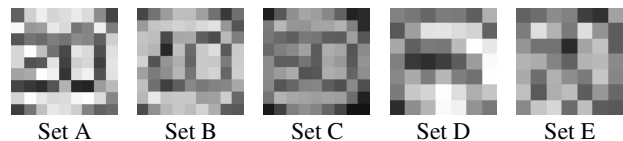
Set	Category	Number of symbol images in video data	
		For each individual sign	Total
A	No.2	95 + 79	174
B	No.4	117 + 55 + 69 + 44 + 71	356
C	No.5	77 + 67 + 70	214
D	No.12	110 + 59 + 45	214
E	No.20	69 + 46	115

subspace is well trained using parameters estimated from different category sets. Images in which signs were not detected or improperly segmented were manually excluded from the data sets. Table 3 shows these data sets (sets A–E) and the number of their symbol images successfully detected by the algorithm in 4.3. In this experiment, each data set was chosen for parameter estimation, and the remaining four sets were used for testing. In other words, each bit of data was evaluated as test data by changing the training data four times using the round-robin method. Figure 9 shows the distribution of the segmented image's size, and Fig. 10 shows examples of the test data.

In the training step, the parameter estimation algorithm in Appendix was applied with $N_c = 100$, $G = 100$, $P_c = 0.7$, and $P_m = 0.01$. Instead of Eq. (12), training data were generated using a parameter producing function in which $\Sigma^{1/2}$ was weighted on as

$$\mathbf{g} = k\Sigma^{1/2}\mathbf{r} + \boldsymbol{\mu}, \quad (20)$$

where k is considered as a factor that controls the parameter

**Fig. 9** Distribution of traffic sign size.**Fig. 10** Examples of test data.

range of the training set by weighting on the estimated $\Sigma^{1/2}$. The number of the generated training data was 200 ($N = 200$). Recognition rates in six cases ($k = 0, 1/4, 1/2, 1, 2, 4$) were compared. In the case of $k = 0$, however, a single training datum was generated from Eq. (20). Hence in this case, the test data were classified by

$$\hat{c} = \arg \max_c \sum_{m=1}^M \langle \mathbf{x}_{\bar{d}_m}^{(c)}, \mathbf{z}_m \rangle \quad (21)$$

with training datum $\mathbf{x}_{\bar{d}_m}^{(c)}$. In the other cases, recognition results were obtained by Eq. (15). The case of $k = 1$ was identical to the proposed method, since Eq. (20) equals Eq. (12). In the recognition step, ten successive frames were used for multiple frame integration ($M = 10$), and ten eigenvectors were used ($L = 10$).

5.1 Results

Recognition rates are presented in Fig. 11 and Table 4, where the horizontal axis in the graph represents the maximum symbol size \bar{d}_{\max} within the integrated M frames. As shown in the results, the recognition rates have strong relationships with symbol sizes. In the case of the proposed method, the recognition rate of relatively large symbols ($\bar{d}_{\max} \geq 20$) was 100% and 84.4% for small symbols ($\bar{d}_{\max} < 10$). Compared with the case of $k = 0$, in which similarity to an average pattern was evaluated, the recognition rates were drastically improved. Although the other cases of k ($k = 1/4, 1/2, 2, 4$) also exhibited high recognition rates, the case of $k = 1$ was the most effective.

5.2 Discussion

Note that the case using estimated distributions ($k = 1$) was

Table 5 Recognition rates of proposed method ($k = 1$) for each training and test set.

Estimation data	Recognition rates for test data [%]						
	Single frame						Multiple frames Average
	Set A	Set B	Set C	Set D	Set E	Average	
Set A	97.1	68.0	68.2	98.6	100	82.3	93.5
Set B	97.7	78.4	72.0	100	100	86.9	95.8
Set C	93.7	82.6	82.7	100	100	89.7	98.5
Set D	91.4	83.1	65.4	98.6	100	85.8	91.5
Set E	89.1	76.4	56.1	98.1	100	81.3	90.0

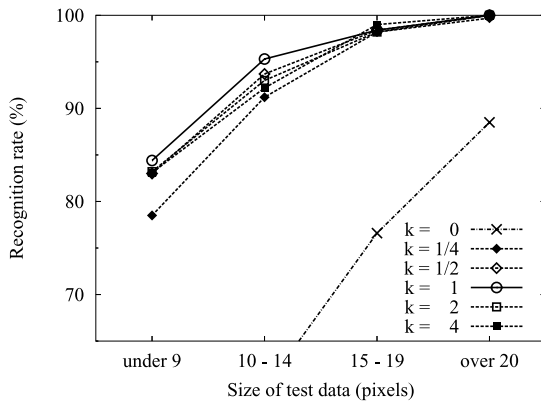


Fig. 11 Recognition results according to maximum size of symbol image in multiple frames.

Table 4 Average recognition rates from single frame and multiple frame integration ($M = 10$).

k	0	1/4	1/2	1	2	4
Single frame	48.0	81.7	83.4	84.3	82.7	82.4
Multiple frames	57.4	89.2	91.7	92.9	91.4	91.2

the most appropriate for recognizing signs captured in similar conditions. This result indicates that GA-based parameter estimation successfully worked and also exhibited the superiority of the proposed method over the other k s.

Since most of the available sign images are small, as shown in Fig. 9, robustness to the low-resolution case is important for realworld applications. Nevertheless, the recognition rate was not high enough where the test data were of very small size ($\bar{d}_{max} < 10$). One reason is that small signs are especially sensitive to the degradation factors. This implies the dependency of parameters, which are listed in Eq. (9), on size parameter d . For simplicity in simulations, the proposed method assumes independence of d from the other parameters. A better representation for parameter distribution must also be discussed in future work.

Table 5 shows the recognition rates of the proposed method ($k = 1$) for each data set. A sufficient performance should be obtained also from the case where different sets were used for estimation and testing (non-diagonal elements in Table 5). Compared with the case where the same set was used both for estimation and testing, however, they did not exhibit high recognition rates, when sets A and C were tested. This is partly due to the distribution of traffic sign

Table 6 Edge density of traffic sign symbols. They are measured from original symbol images of 56×56 pixels.

Set	A	B	C	D	E
Category	No.2	No.4	No.5	No.12	No.20
Edge density	0.064	0.061	0.065	0.046	0.055

size in Fig. 9; set A was composed mostly of large images, and set C was composed mostly of small images. Moreover, the results were less satisfactory when sets D and E were used for parameter estimation. One explanation is that the performance of the GA-based parameter estimation was relatively low because of structural simplicity of the original traffic sign symbols. Table 6 shows the complexities calculated for the traffic sign symbols, where the complexity is defined by edge density as introduced in [27]. Altogether, parameters should preferably be estimated using structurally complex symbols and images of various sizes.

6. Conclusion

In this paper, a method for recognizing traffic sign symbols was proposed. Degradation parameters were defined to simulate actual degradations. Based on the defined model, degradation characteristics were estimated from a small number of captured images for training, and training data for all categories were generated. The usefulness of our method for degraded traffic sign images was experimentally demonstrated.

The proposed method is applicable for any sign by combining it with other traffic sign detection methods [4]–[14]. As for future research, the effectiveness of the method should be evaluated under various weather conditions and at various times of day. Generation-based approaches also for detecting other traffic objects will be interesting for future consideration.

Acknowledgements

Parts of this research were supported by the Grant-In-Aid for Scientific Research (16300054) and the 21st century COE program from the Ministry of Education, Culture, Sports, Science and Technology. This work was developed based on MIST library (<http://mist.suenaga.m.is.nagoya-u.ac.jp/>).

References

[1] D. Mochiduki, Y. Yano, T. Hashiyama, and S. Okuma, "Pedestrian

- detection with a vehicle camera using fast template matching based on background elimination and active search,” IEICE Trans. Inf. & Syst. (Japanese Edition), vol.J87-D-II, no.5, pp.1094–1103, May 2004.
- [2] F. Lindner, U. Kressel, and S. Kaelberer, “Robust recognition of traffic signals,” Proc. IEEE 2004 Intelligent Vehicle Symp., pp.49–53, Parma, Italy, June 2004.
- [3] H. Kurihata, T. Takahashi, Y. Mekada, I. Ide, H. Murase, Y. Tamatsu, and T. Miyahara, “Rainy weather recognition from in-vehicle camera images for driver assistance,” Proc. IEEE 2005 Intelligent Vehicle Symp., pp.204–209, Las Vegas, USA, June 2005.
- [4] A. Escalera and M. Salichs, “Road traffic sign detection and classification,” IEEE Trans. Ind. Electron., vol.44, no.6, pp.848–859, Dec. 1997.
- [5] D. Gavrilu, “Multi-feature hierarchical template matching using distance transforms,” Proc. IEEE 14th Int. Conf. on Pattern Recognition, vol.1, pp.439–444, Brisbane, Australia, Aug. 1998.
- [6] J. Miura, T. Kanda, and Y. Shirai, “An active vision system for real-time traffic sign recognition,” Proc. IEEE Intelligent Transportation Systems, Dearborn, USA, pp.52–57, June 2000.
- [7] G. Mo and Y. Aoki, “A recognition method for traffic sign in color image,” IEICE Trans. Inf. & Syst. (Japanese Edition), vol.J87-D-II, no.12, pp.2124–2135, Dec. 2004.
- [8] K. Uchimura, H. Kimura, and S. Wakiyama, “Extraction and recognition of circular road signs using road scene color images,” IEICE Trans. Fundamentals (Japanese Edition), vol.J81-A, no.4, pp.546–553, April 1998.
- [9] D. Matsuura, H. Yamauchi, and H. Takahashi, “Extracting circular road signs using specific color distinction and region limitation,” IEICE Trans. Inf. & Syst. (Japanese Edition), vol.J85-D-II, no.6, pp.1075–1083, June 2002.
- [10] S. Lafuente-Arroyo, P. Gil-Jimenez, R. Maldonado-Bascon, and F. Lopez-Ferreras, “Traffic sign shape classification evaluation I: SVM using distance to borders,” Proc. IEEE 2005 Intelligent Vehicles Symposium, pp.557–562, Las Vegas, USA, June 2005.
- [11] P. Gil-Jimenez, S. Lafuente-Arroyo, H. Gomez-Moreno, F. Lopez-Ferreras, and S. Maldonado-Bascon, “Traffic sign shape classification evaluation II: FFT applied to the signature of blobs,” Proc. IEEE 2005 Intelligent Vehicles Symposium, pp.607–612, Las Vegas, USA, June 2005.
- [12] C. Bahlmann, Y. Zhu, V. Ramesh, M. Pellkofer, and T. Koehler, “A system for traffic sign recognition, tracking, and recognition using color, shape, and motion information,” Proc. IEEE 2005 Intelligent Vehicles Symposium, pp.255–260, Las Vegas, USA, June 2005.
- [13] B. Johansson, Road sign recognition from a moving vehicles, Master’s thesis, Center for Image Analysis, Swedish University of Agricultural Science, 2002.
- [14] P. Paclik, J. Novovicova, and R. Duin, “Building road sign classifiers using trainable similarity measure,” IEEE Trans. Intelligent Transportation Systems, vol.7, no.3, pp.293–308, Sept. 2006.
- [15] L. Daris, Handbook of genetic algorithms, Van Nostrand Reinhold, New York, 1991.
- [16] E. Oja, Subspace methods of pattern recognition, Research Studies, Hertfordshire, UK, 1983.
- [17] H. Murase and S. Nayar, “Learning by a generation approach to appearance-based object recognition,” Proc. 13th Int. Conf. on Pattern Recognition, pp.24–29, Vienna, Austria, Aug. 1996.
- [18] K. Ishii, “Generation of distorted characters and its applications,” Systems and Computers in Japan, vol.14, no.6, pp.19–27, June 1983.
- [19] T. Horiuchi, K. Toraichi, L. Yamamoto, and H. Yamada, “On method of training dictionaries for handwritten character recognition using relaxation matching,” Proc. 2nd Int. Conf. on Document Analysis and Recognition, pp.638–641, Tsukuba, Japan, Oct. 1993.
- [20] H. Ishida, S. Yanadume, T. Takahashi, I. Ide, Y. Mekada, and H. Murase, “Recognition of low-resolution characters by a generative learning method,” Proc. 1st Int. Workshop on Camera-Based Document Analysis and Recognition, pp.45–51, Seoul, Korea, Aug. 2005.
- [21] H. Ishida, T. Takahashi, I. Ide, Y. Mekada, and H. Murase, “A generative learning method for the recognition of blurred characters taken by portable cameras,” IEICE Trans. Inf. & Syst. (Japanese Edition), vol.J89-D, no.9, pp.2055–2064, Sept. 2006.
- [22] J. Sun, Y. Hotta, Y. Katsuyama, and S. Naoi, “Camera based degraded text recognition using grayscale feature,” Proc. 8th Int. Conf. on Document Analysis and Recognition, pp.182–186, Seoul, Korea, Aug. 2005.
- [23] J. von Neumann, “Various techniques used in connection with random digits,” National Bureau of Standards Series, no.12, pp.36–38, 1951.
- [24] G. Golub and C. Loan, Matrix computations, 2nd ed., Johns Hopkins Press, 1992.
- [25] S. Yanadume, Y. Mekada, I. Ide, and H. Murase, “Recognition of very low-resolution characters from motion images,” Proc. PCM2004, Lecture Notes in Computer Science, vol.3331, pp.247–254, Springer-Verlag, Dec. 2004.
- [26] A. Smith, “Color Gamut transform pairs,” Computer Graphics, vol.12, no.3, pp.12–19, Aug. 1978.
- [27] K. Hirayama, S. Omachi, and H. Aso, “String extraction from scene images using color and luminance information,” IEICE Trans. Inf. & Syst. (Japanese Edition), vol.J89-D, no.4, pp.893–896, April 2006.

Appendix: Parameter Estimation Algorithm

Algorithm

```

//  $C_p$ : Parents set
//  $C_c$ : Children set
//  $t$ : Normalized captured image  $T$ 
//  $q$ : Normalized generated image  $Q$ 
1 initialize set  $C_p$  and its  $N_c$  chromosomes  $p_i$ 
2 do
3   for all  $p_i \in C_p$ 
4     generate  $q_i$  from the original image of  $t$  with  $p_i$ 
5     calculate fitness  $s_i = \langle q_i, t \rangle$ 
6   next
7   do
8     select chromosomes  $p_a, p_b$  by roulette selection
9     reproduce  $p_a \rightarrow p'_a, p_b \rightarrow p'_b$ 
10    /* Crossover */
11    if Rand[0, 1) <  $P_c$  then cross  $p'_a$  with  $p'_b$ 
12    add  $p'_a, p'_b$  to  $C_c$ 
13  until  $|C_p| = |C_c|$ 
14  for each chromosome  $p_i$  of  $C_c$ 
15    /* Mutation */
16    if Rand[0, 1) <  $P_m$  then
17      randomly initialize one of the elements of  $p_i$ 
18  next
19  copy  $C_c \rightarrow C_p$ 
20  empty  $C_c$ 
21 until generation reaches  $G$ 
22  $\hat{p} := p_i$  with the largest fitness  $s_i$ 
23 return  $\hat{p}$ 

```



Hiroyuki Ishida received his B.S. and M.S. degrees from the Department of Information Engineering and from the Graduate School of Information Science, respectively, at Nagoya University. He is currently pursuing a Ph.D. in Information Science at Nagoya University.



Tomokazu Takahashi received his B.S. degree from the Department of Information Engineering at Ibaraki University, and his M.S. and Ph.D. from the Graduate School of Science and Engineering at Ibaraki University. His research interests include computer graphics and image recognition.



Ichiro Ide received his B.S. degree from the Department of Electronic Engineering, his M.S. degree from the Department of Information Engineering, and his Ph.D. from the Department of Electrical Engineering at The University of Tokyo. He is currently an Associate Professor in the Graduate School of Information Science at Nagoya University.



Yoshito Mekada received his B.S., M.S., and Ph.D. degrees from the Graduate School of Information Engineering at Nagoya University. He is currently a Professor in the School of Life System Science and Technology at Chukyo University.



Hiroshi Murase received his B.S., M.S., and Ph.D. degrees from the Graduate School of Electrical Engineering at Nagoya University. He is currently a Professor in the Graduate School of Information Science at Nagoya University. He received the Ministry Award from the Ministry of Education, Culture, Sports, Science and Technology in Japan in 2003. He is a Fellow of the IEEE.